Article

JOURNAL OF COMPOSITE MATERIALS

Journal of Composite Materials
2015, Vol. 49(24) 3057–3066

DOI: 10.1177/0021998314559279
jcm.sagepub.com

SAGE

Mechanical properties of C–SiC composite materials fabricated by the Si–Cr alloy melt-infiltration method

Seyoung Kim[1,2], In Sub Han[2], Young-Hoon Seong[2] and Do Kyung Kim[1]

Abstract

Although carbon fiber-reinforced silicon carbide matrix composites fabricated using the liquid silicon infiltration method exhibit high thermal and oxidation resistances, their physical characteristics are limited because of the presence of unreacted, free Si within the materials. To resolve this problem, ingots prepared by alloying Cr with Si in ratios of 0, 5, 10, 25, and 50 at% were melted and made to infiltrate the composite, resulting in the formation of $CrSi_2$ in the unreacted, free Si region without degrading the composite's properties. The $CrSi_2$ in the composite material reduced the amount of free Si and caused minimal variation in the flexural strength while significantly improving the fracture toughness of the composite. The results of scanning electron microscopy and transmission electron microscopy analyses indicated that the improvement in the fracture toughness was due to the presence of an amorphous interlayer between the Si and $CrSi_2$ phases, as well as because of a stress field surrounding the $CrSi_2$ phase.

Keywords

LSI, $CrSi_2$, ceramic matrix composite, fracture toughness

Introduction

Carbon fiber-reinforced silicon carbide matrix (C/SiC) composites, which exhibit high resistances against heat and oxidation, as well as better mechanical properties than those of monolithic SiC, are widely used in a number of fields, including in the defense and aerospace industries.[1–3] There are several techniques for fabricating such composites, including chemical vapor infiltration (CVI) and polymer impregnation and pyrolysis (PIP). However, the liquid silicon infiltration (LSI) method is garnering a lot of attention. Because the process is a quick and low-cost one, a diverse range of products can be manufactured using the LSI technique. While CVI and PIP processes involve long processing times and encounter dimensional limitations, the LSI method does not result in material shrinkage. In addition, thick, large-scale, and pore-free products can be fabricated using the method. The fabrication of C/SiC composites using the LSI process involves the following two stages. The first step is to produce a porous carbon fiber–carbon (C/C) preform, and the second is to make molten Si infiltrate the preform at a temperature of 1420°C or higher.[4–8] The infiltrated Si reacts with the carbon, forming facet-shaped, stable α-SiC at the high temperature and increasing the internal density. However, 10–14% of the unreacted, free Si that does not participate in the reaction with the carbon remains inside the composite.[9–13] In general, this unreacted, free Si degrades the mechanical and thermal characteristics of the composite. The working temperature of LSIed composites is limited to 1350°C because of the softening of the unreacted, free Si that is present in their microstructure and the brittle properties of Si inhibit good mechanical characteristics. Fracture toughness (K_{IC}) of Si is about 1 MPa$m^{1/2}$, which is lower than

[1]Department of Materials Science and Engineering, Korea Advanced Institute of Science and Technology (KAIST), South Korea
[2]Energy Materials Laboratory, Korea Institute of Energy Research (KIER), South Korea

Corresponding author:
Do Kyung Kim, Department of Materials Science and Engineering, Korea Advanced Institute of Science and Technology (KAIST), 291 Daehak-ro, Yuseong-gu, Daejeon, South Korea.
Email: dkkim@kaist.ac.kr

average engineering ceramic's 3 MP am$^{1/2}$.[14–20] Various methods have been investigated for reducing free Si in LSIed composite to overcome this problem including controlling the pore dimensions of the C/C preform and alloy high-temperature Si alloy infiltration.[21,22] Esfehanian employed two different disilicides—$MoSi_2$ and $TiSi_2$—during the LSI process and found that composites could be fabricated successfully by alloy infiltration without causing substantial damage to the fibers.[22] Zhu reported the possibility of improving the material characteristics of conventional reaction-bonded SiC through alloy infiltration by fabricating SiC-$Mo_5(Si,Al)_3C$ using the melt-infiltration method and increasing its K_{IC} value to 1400°C.[23] As such, there is active research underway on other methods to replace the unreacted, free Si with various metals in order to improve the composite characteristics. The silicides of transition metals (groups IVa–VIa in the periodic table) have been the focus of particular interest as high-temperature structural materials.[24] In this context, Cr is one of the materials being explored. Cr reacts with Si to form $CrSi_2$, which has a high strength. It also reacts with C to form CrC. Therefore, employing Si and Cr during the LSI process results in the formation of $CrSi_2$ and CrC, which are superior to the unreacted, free Si in terms of thermal and mechanical characteristics and improve composite properties. Furthermore, of the various silicides being investigated, $CrSi_2$ has a relatively low density at 5.02 g cm^{-3}, which results in a decrease in the final product's weight.

In this study, Si–Cr alloys were used during the LSI process instead of Si to allow a Si–Cr alloy phase to be formed in the region where the unreacted, free Si had existed previously. The objective was to improve the mechanical properties and the fracture toughness of conventional LSIed composites. The mechanism responsible for the improvements was also investigated.

Materials and methods

Si–Cr ingot preparation

Si–Cr ingots were prepared by mixing powders of Si (particle size: 8 μm, grade 2, Sicomill, Vestaceramic, Sweden) and Cr (particle size: 74 μm, Junsei, Japan) in ratios of 0, 5, 10, 25, 50 at%; these mixtures (and the corresponding composites) were labeled as Cr0, Cr5, Cr10, Cr25, and Cr50, respectively. The mixed powders were then melted in an induction furnace under 300 mTorr of vacuum atmosphere. The powders were melted completely and were confirmed through a quartz inspection window and formation of CrSi2 phase in alloy ingot was observed by SEM with energy-dispersive X-ray spectroscopy (EDX) inspection. The obtained alloy ingots were then cut into 1 × 1 × 1 cm cubes for the experiments.

Composite fabrication

Plain, woven polyacrylonitrile-based carbon fabric (T300-12 K, Toray, Japan) was used as the reinforcement fiber. After laminating 20 plies of the fabric, phenol resin (KRD-HM2, Kolon Chem., South Korea) was made to impregnate the laminate using the vacuum-assisted resin transfer molding process. The impregnated laminate was cured at 120°C and subjected to a carbonizing process at 1900°C in a nitrogen atmosphere to produce a porous C/C preform. All the composites used in this study were obtained by melting the ingots of different compositions and make them infiltrate the porous C/C preform at temperatures of 1600°C or greater.

Specimen preparation

The C/SiC–$CrSi_2$ composites produced using the various alloy ingots were made into modulus of rupture (MOR)-shaped bars for flexural strength and fracture toughness evaluation. The specimens for measuring the flexural strength had dimensions of 3 × 4 × 50 mm, and their cut cross sections and edges were chamfered using sandpaper. The K_{IC} specimens used for measuring the fracture toughness had dimensions of 4 × 3 × 50 mm. Their initial cracks were processed using a razor blade and a 0.25-μm diamond suspension. Single edge v-notched beam (SEVNB) specimens with initial cracks with a size of 0.4 (= a/W, a: crack length and W: width of specimen), and very sharp crack tips were obtained.

Evaluation methods

Variations in the densities and porosities of the composite specimens with changes in the Cr content of the Si–Cr alloy used were measured using Archimedes' principle. The components of C/SiC–$CrSi_2$ for each composition were analyzed using X-ray diffraction (XRD) analysis (Dmax-2500PC, Rigaku, Japan). The flexural strengths of the samples were measured using the 4-point method. A universal testing machine (Landmark, MTS, USA) with an inner span of 20 mm, an outer span of 40 mm, and a crosshead speed of 1 mm min^{-1} was employed for the purpose. The same procedure was also used for the K_{IC} value measurements. The average values of 10 measurements were calculated. In addition, the samples were analyzed using scanning electron microscopy (SEM) (S-4800, Hitachi, Japan) to inspect their microstructures and to check for crack propagation. In order to elucidate the role of Cr in determining the flexural strengths and

the fracture toughness of the composites infiltrated with the Si–Cr alloys, a focused ion beam was used to prepare transmission electron microscopy (TEM) specimens; these specimens contained a Si–Cr alloy interphase region. The specimens were analyzed using a 300-kV TEM system (Tecnai G^2 F30 S-Twin, FEI, USA).

Results and discussion

Si–Cr alloy-infiltrated composites

Figure 1 shows SEM images of the cross section of composite sample after a Si–Cr alloy had been melted and made to infiltrate the porous C/C preform. It can be seen that the alloy reacted with the carbon inside the preform to produce crystalline SiC. In particular, it could be confirmed that Si and Cr regions coexisted in the unreacted, free Si phase that had been formed when only Si had infiltrated the preform. The Si–Cr alloy phase was evenly distributed in the fiber bundle and was present in various shapes and sizes. As can be seen from the SEM images, when an alloy containing an optimum amount of Cr was made to infiltrate the preform during the LSI process, the molten alloy is still sufficient to infiltrate the preform meaning that wetting angle was below 90°. It was also confirmed that a new secondary phase was formed in the region of the unreacted, free Si.

Figure 2 shows the XRD patterns of three composites, one infiltrated with Si and two infiltrated with 10 and 25% Si–Cr alloys. In the case of the Si-infiltrated composite, the phases observed were those of carbon, silicon carbide, and Si. In addition to these phases, the composites infiltrated with the 10 and 25% Si–Cr alloys also exhibited a $CrSi_2$ phase. These results indicate that Si–Cr alloys can be used to manufacture fiber-reinforced composites using the melt-infiltration process. Moreover, it was also confirmed that a Si–Cr alloy with a stoichiometric composition was formed within the infiltrated composites. $CrSi_2$ has a C40 hexagonal structure and a density of 5.02 g cm^{-3}, which is lower than that of most disilicides. The Young's modulus of $CrSi_2$ is 350 GPa, which is higher than that of Si (112 GPa).[15,25] The intensity of the peak corresponding to Si decreased with an increase in the Cr content, indicating that the formation of the $CrSi_2$ phase reduced the amount of unreacted, free Si; this was expected to improve the mechanical properties of the composite. However, the XRD analysis results did not indicate the presence of carbides composition with Cr. This is because the $\Delta G_{f\blacksquare reaction}$ value at the alloy melt-infiltration temperature (1773 K) was 128 kJ Mol^{-1} and not suitable to allow the reaction shown below to occur and for chromium carbide to be formed.

$$3CrSi_2 + 2C \rightarrow Cr_3C_2 + 6Si \quad (1)$$

$CrSi_2$ was produced only when an ingot of an alloy of Si and Cr was formed and then melted and made to infiltrate into the preform instead of molten Si. This also prevented other chromium carbides from forming. In turn, it was confirmed that only carbon, silicon carbide, $CrSi_2$, and a limited amount of unreacted, free Si existed in the thus-fabricated sample.

Once the Cr–Si alloy was inside the sample, its density and porosity changed. The extent of the change was dependent on the Cr content, and the results are shown in Figure 3. The composite that did not contain Cr had a density of 2.2 g cm^{-3}, which increased only by a little to 2.3 g cm^{-3} after the addition of 10% Cr. Similarly, the open porosity remained within 2.5% and did not

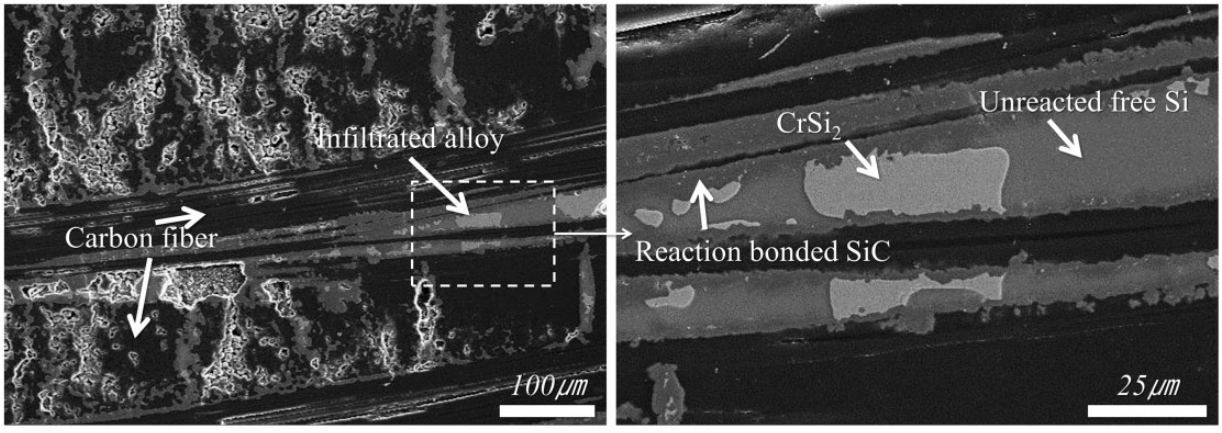

Figure 1. Cross-sectional micro structure of Si–Cr alloy infiltrate composite with $CrSi_2$ in matrix (right: magnification showing the marked square region of left figure).

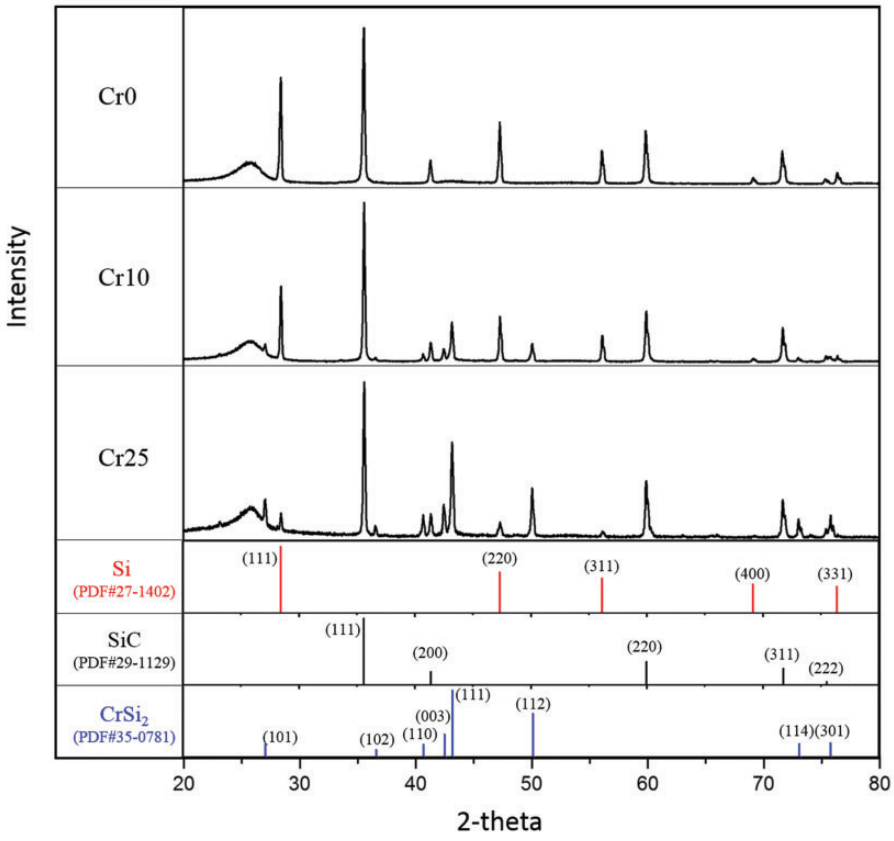

Figure 2. XRD patterns of Si–Cr alloy-infiltrated composite material.

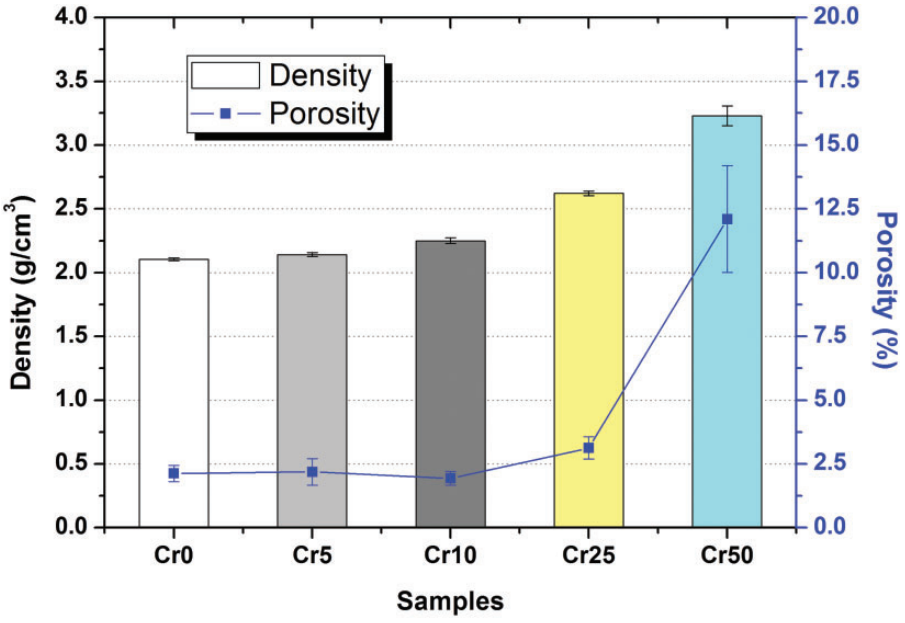

Figure 3. Density and porosity result after Si–Cr alloy-infiltrated composite materials.

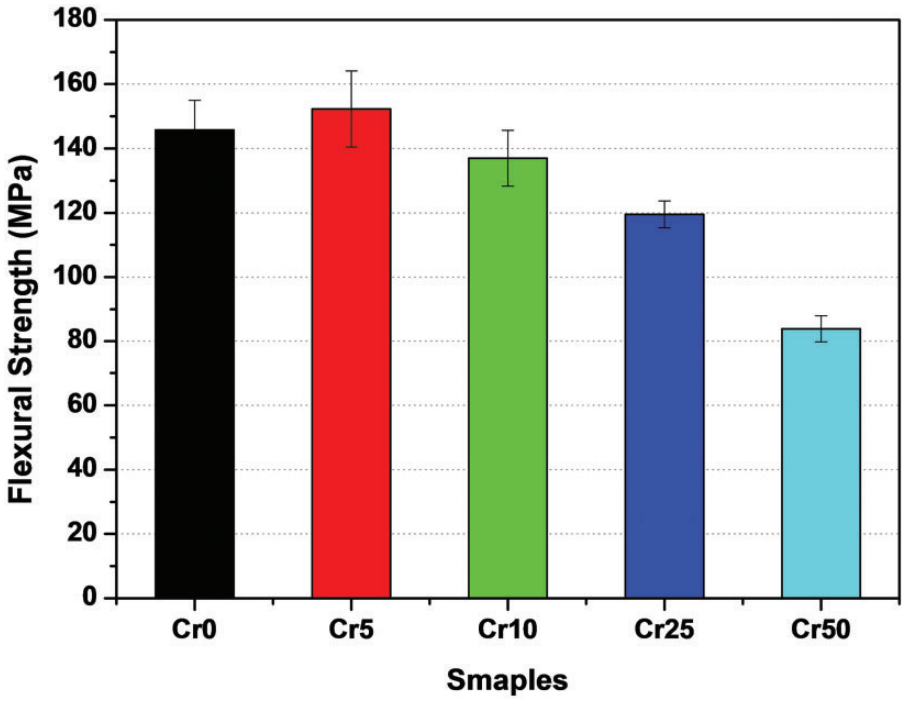

Figure 4. Flexural strength result after Si–Cr alloy-infiltrated composite materials.

vary much even after the addition of 10% Cr, indicating that the fabricated composite was very dense.

However, for Cr contents of 25% and higher, the density increased significantly. When the Cr content was 50%, the density increased to $3\,g\,cm^{-3}$ and the porosity to 12.5%. Because the density of Cr is approximately $5.02\,g\,cm^{-3}$ and much higher than that of Si ($2.3\,g\,cm^{-3}$), the density of the Cr-containing composites increased in proportion to the amount of Cr present, in keeping with the rule of mixtures. The composites with 25% or more Cr contained a large number of pores. In particular, Cr50 showed a high mean porosity with a significant standard deviation; this was indicative of the very low reliability of the composite. In other words, no major problems were encountered during the LSI process when using the Si-rich Si–Cr alloys maintaining low porosity. However, the porosity increased when using Cr-rich Si–Cr alloys.

Mechanical properties of the Si–Cr alloyed composites

Figure 4 shows the average flexural strengths with standard deviation of the composites fabricated using the Si–Cr alloys with the different Cr contents. The flexural strength of the Cr-free composite was 145 MPa and slightly increased to 150 MPa in the case of the composite with a Cr content of 5%. However, when the Cr content was increased further, the flexural strength did not increase but decreased instead to a level lower than the initial strength of the Cr-free sample. In other words, the presence of Cr did not significantly increase the flexural strength. From these results, it could be determined that flexural strength of the composites was not affected significantly by the formation of $CrSi_2$. Adding up to 5% Cr improved the flexural strength by a little because when a second phase with better strength characteristics is reinforced in a typical ceramic material, the flexural strength of the material improves to a certain degree.[26] However, as mentioned previously, there was little difference in the flexural strengths of Cr0, Cr5, and Cr10. Further, as mentioned previously, adding 25% or more Cr significantly increased the internal porosity, decreasing the composite's mechanical properties. Accordingly, Cr50, which had a porosity of more than 12%, had a very low flexural strength at 80 MPa.[27]

The fracture toughness of fiber-reinforced ceramic composites is a material characteristic that receives more attention than does strength. As mentioned earlier, in this study, tests were performed on samples prepared by the SEVNB method to investigate the fracture toughness characteristics of the various composite samples as well as the underlying strengthening mechanism. Whereas increasing the Cr content did not improve the flexural strength, there were significant changes in the case of the fracture toughness. These results are shown in Figure 5. The fracture toughness of the Cr-free composite was $2.4\,MPa\,m^{1/2}$, which increased by 1.7 times

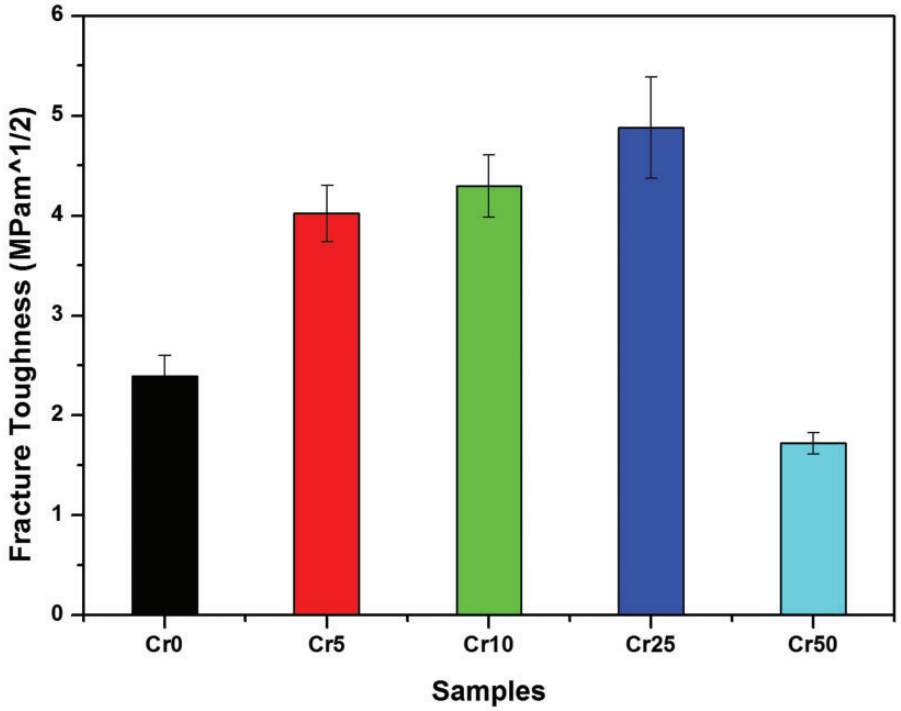

Figure 5. Fracture toughness result of SEVNB specimen after Si–Cr alloy-infiltrated composite materials.

to approximately 4 MP am$^{1/2}$ in the case of the specimen containing 5% Cr. The fracture toughness kept increasing for Cr contents as high as 25%, but decreased markedly when the content was 50% Cr. There have been reports that, for a few ceramic materials, pores have a positive effect in terms of the fracture toughness because crack tip blunting occurs when a crack encounters voids, and this reduces the stress concentration.[28] Cr25 exhibited good fracture toughness because it contained a larger amount of $CrSi_2$ than did the other specimens, as well as a few pores. However, in the case of Cr50, the standard deviation of the porosity was too high, and the aforementioned improvement in the fracture toughness resulting from an optimum amount of pores being present did not occur. The stress concentration on loading surface can be generated by surface pores that reduce the crack-opening resistance when sample has large amount of porosity. It is also likely that the damage caused to the internal fibers by infiltration of alloys with a high Cr content drastically reduced the fracture toughness. Whereas increasing the Cr content did not result in significant improvements in the flexural strength, it did increase the fracture toughness substantially. In contrast to the reduction seen in its flexural strength, Cr25 exhibited the highest fracture toughness. This confirmed that the presence of $CrSi_2$ within the composite matrix improved the resistance against crack formation and crack propagation more than it did the composite strength.

The mechanism underlying the improvements seen in the fracture toughness became clear when we examined the SEM images of a region of crack propagation, as shown in Figure 6. As can be seen from Figure 6(a), cracks generally propagated in a nearly straight line in the regions containing only the unreacted, free Si, subsequently moving to the fiber bundles or the reacted SiC phase. On the other hand, in the region shown in Figure 6(b), where $CrSi_2$ coexisted with the unreacted, free Si, the propagating cracks encountered a region rich in $CrSi_2$, which prevented the cracks from propagating in a straight line, resulting in crack bridging.

As mentioned earlier, $CrSi_2$ has a C40 hexagonal structure and the highest critical shear stress measured of all the silicides, because slips caused by external forces are not observed in it at temperatures lower than 700°C.[24] This is the reason that $CrSi_2$ acted as an impediment in the crack propagation path. Other reasons for crack bridging and deflection are thermal expansion and residual stress. When there are two phases present, the differences in their thermal expansion rates causes a residual stress to exist in the interphase between the phases. This varies the crack patterns in the interphase. The residual outward pressure from the thermal expansion between the second phase and the matrix can be defined as follows:

$$\sigma_R = \Delta\alpha\Delta T/[(1+\nu_{Si})/2E_{Si} + (1-2\nu_{CrSi2})/E_{CrSi2}] \quad (2)$$

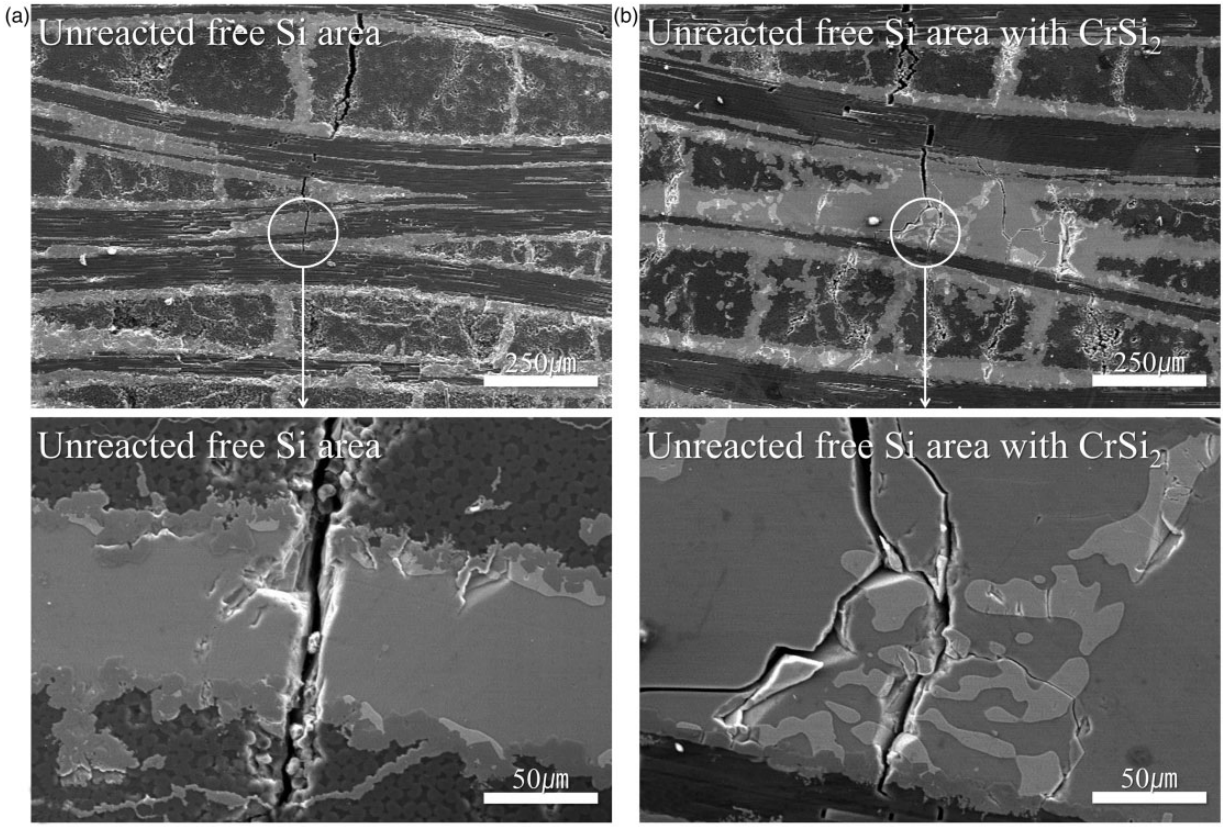

Figure 6. Crack deflection inducement by $CrSi_2$ in composite matrix (a) without $CrSi_2$ (b) with $CrSi_2$.

where $\Delta\alpha = \alpha_{Si} - \alpha_{CrSi2}$, and ΔT is the temperature between solidification of the melt phase and ambient temperature, ν is the Poisson's ratio, and E is the Young's modulus. When $\Delta\alpha > 0$ and $\Delta\alpha < 0$, hoop-tension and radial-tension stress fields are generated, respectively. Depending on lattice direction, the coefficient of thermal expansion of $CrSi_2$ is determined to be 8.9×10^{-6}–$2.5 \times 10^{-5} {}^{\circ}C^{-1}$, which is greater than that of Si (2.5–$4.4 \times 10^{-6} {}^{\circ}C^{-1}$). Therefore, when a composite is fabricated at a high temperature and cooled to room temperature, $\Delta\alpha < 0$ between $CrSi_2$ and Si, creating a radial-tension field around the $CrSi_2$ phase. As shown in Figure 6(b), the stress field-induced crack propagation, and the cracks deflected around $CrSi_2$ in several paths rather than penetrating it. This was the major factor behind the improvement in the fracture toughness of the composites.[15,29]

While it was confirmed that the increase in the fracture toughness was due to crack propagation being impeded in the unreacted, free Si region where $CrSi_2$ existed, TEM analysis was performed to investigate the mechanism of crack deflection. The results of the analysis are shown in Figure 7. The TEM analysis was performed on the interphase between $CrSi_2$ and Si that existed in the unreacted, free Si region. The dark and bright areas of Figure 7 (a) represent the $CrSi_2$ and Si regions, respectively. According to the results of the selected area electron diffraction (SAED) analysis of the interphase, a crystalline $CrSi_2$ phase was formed, with clear diffraction patterns corresponding to the (1 0 0) and (2 0 1) planes being observed. The interplane distances were 3.83 Å and 2.43 Å, respectively. A crystal Si phase was also formed, with clear diffraction patterns corresponding to the (2 2 0) and (4 0 0) planes being observed. The interplane distances in this case were 1.90 Å and 1.36 Å, respectively. The results of TEM/EDX, shown in Table 1, suggested that the regions consisted of (b) $CrSi_2$, (c) small amounts of Cr and Si, and (d) Si, confirming the aforementioned hypothesis. Therefore, it could be confirmed that fabricating a composite by making both Cr and Si infiltrate it simultaneously results in the formation of $CrSi_2$, which has a C40 hexagonal structure. At the same time, it was also observed that an interlayer existed between $CrSi_2$ and Si. As indicated by the TEM/EDX results shown in Table 1, the primary component was Si; however, a small amount of Cr was also present. In addition, no clear pattern was observed during the SAED analysis of the TEM images, confirming that an amorphous-phase interlayer existed between the crystals of $CrSi_2$ and Si. Since the amorphous phase has atomic disordering that lower elastic modulus and

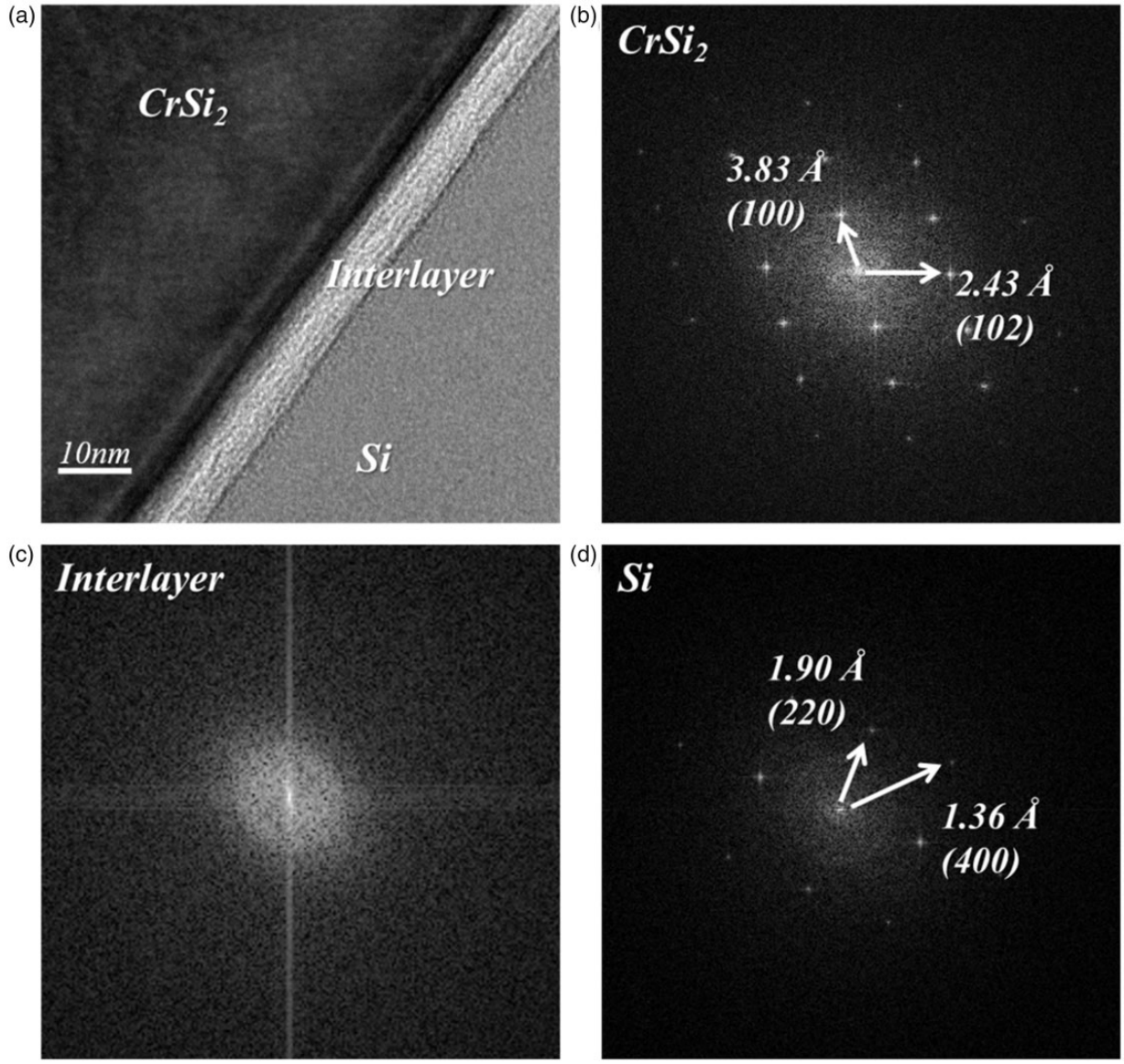

Figure 7. TEM image (a) and SAED patterns (b, c and d).

Table 1. Element analyses result from TEM.

Atomic %	$CrSi_2$	Interlayer	Si
Si	60.1	94.9	100.0
Cr	39.9	5.1	0.0

Note: TEM, transmission electron microscopy.

strength than crystalline Si, this amorphous interlayer had a strength lower than the high deformation energy of the hexagonal-structured $CrSi_2$.[30] Therefore, the crack can propagate through interlayer between Si and $CrSi_2$.

Conclusions

In order to reinforce the brittle, unreacted, and free Si that remains within the matrix of composites fabricated using the LSI process, molted Cr–Si alloys were made to infiltrate the composite instead, resulting in carbon fiber-reinforced ceramic composites containing Cr in amounts of 5–50% in place of Si.

It was confirmed that $CrSi_2$ was formed within the fabricated composites in the regions where only the unreacted, free Si existed. The flexural strength increased slightly with an increase in the Cr content; however, the fracture toughness improved significantly, from 2.4 MP am$^{1/2}$ to 4.3 MP am$^{1/2}$. The increase in the

fracture toughness could be explained by the results of SEM and TEM analyses. The results of TEM analysis indicated that crystalline $CrSi_2$ was formed within the composite matrix and that there was an amorphous Si interlayer between the unreacted, free Si and $CrSi_2$. In addition, it was confirmed that this weak, amorphous interlayer caused crack bridging and deflection, resulting in cracks not propagating through the $CrSi_2$ phase. The stress field created by thermal expansion played a role in changing the crack propagation behavior and increasing fracture toughness. However, increasing the Cr content increased the porosity, making the composite unsuitable for melt infiltration. It was also determined that there is an optimum composition for improving the flexural strength and fracture toughness through Cr alloy infiltration.

Funding

This work was supported by Korea Evaluation Institute of Industrial Technology and grant funded by Korea Government (Ministry of Trade, Industry, and Energy) under Core Defense Technology Development program (G01201312010100).

Conflict of interest

None declared.

References

1. Krenkel W and Berndt F. C/C–SiC composites for space applications and advanced friction systems. *Mater Sci Eng A* 2005; 412: 177–181.
2. Xu Y, Zhang Y, Cheng L, et al. Preparation and friction behavior of carbon fiber reinforced silicon carbide matrix composites. *Cera Inter* 2007; 33: 439–445.
3. Esfehanian M, Guenster J, Heinrich JG, et al. High-temperature mechanical behavior of carbon–silicide–carbide composites developed by alloyed melt infiltration. *J Euro Cera Soc* 2008; 28: 1267–1274.
4. Jang BK and Sakka Y. Influence of microstructure on the thermophysical properties of sintered SiC ceramics. *J Allo Comp* 2008; 463: 493–497.
5. Lee SP, Katoh Y and Kohyama A. Microstructure analysis and strength evaluation of reaction sintered SiC/SiC composites. *Scr Mater* 2001; 44: 153–157.
6. Kochendörfer R. Ceramic matrix composites from space to earth: the move from prototype to serial production. *Cera Eng Sci Proc* 2001; 22: 11–22.
7. Schulte-Fischedick J, Zern A, Mayer J, et al. The morphology of silicon carbide in C/C–SiC composites. *Mater Sci Eng* 2002; A332: 146–152.
8. Zhang Y, Xiao Z and Wang J. Effect of pyrocarbon content in C/C preforms on microstructure and mechanical properties of the C/C–SiC composites. *Mater Sci Eng* 2009; A502: 64–69.
9. Gadow R. *Die Silizierung des Kohlenstoffs*. PhD Thesis, University of Karlsruhe, GER, 1986.
10. Braue W, Pleger R and Weiss R. The nanoscale microstructure of 2D C/C–SiC ceramic composites processed via silicon capillary impregnation. *Proc 2nd Int Conf High Temp Cera Matrix Comp* 1995: 275–280.
11. Gern F. *Capillary infiltration behavior of liquid silicization from C/C composite*. PhD Thesis, University of Stuttgart, GER, 1995.
12. Schulte-Fischedick J, Seiz S, Lů tzenburger N, et al. The crack development on the micro- and mesoscopic scale during the pyrolysis of carbon fibre reinforced plastics to carbon/carbon composites. *Compos: Part A* 2007; 38: 2171–2181.
13. Bulau JR. AE monitoring for control of carbon-carbon pyrolysis. *Proc IEEE Ultra Symp* 1988; 1057–1063.
14. Fischer DS and Schuh CA. Microstructure and fracture of anomalous eutectic silicon-disilicide composites. *Intermetallics* 2011; 19: 1661–1673.
15. Fischer DS. *Development of in-situ toughened silicon-rich alloys: a new class of castable engineering ceramics*. PhD Thesis, Massachusetts Institute of Technology, USA, 2005.
16. Gilman JJ. Direct measurements of the surface energies of crystals. *J App Phys* 1960; 31: 2208.
17. Jaccodine RJ. Surface energy of germanium and silicon. *J Elec Soc* 1963; 110: 524–527.
18. Gadow R and Fitzer E. Fiber-reinforced silicon carbide. *Am Cer Soc Bull* 1986; 65: 326–335.
19. Forrest CW, Kennedy P and Shennan JV. The fabrication and properties of self-bonded silicon carbide bodies. In: *Proceedings of the fifth Symposium on Special Ceramics, The British Ceramic Research Association* 1972: 99–123.
20. Trantina GG and Mehan RL. High-temperature time-dependent strength of a Si/SiC composite. *J Am Cer Soc* 1977; 60: 177–178.
21. Xua S, Qiao G, Li D, et al. Reaction forming of silicon carbide ceramic using phenolic resin derived porous carbon preform. *J Eur Cer Soc* 2009; 29: 2395–2402.
22. Esfehanian M, Guenster J, Heinrich JG, et al. High-temperature mechanical behavior of carbon–silicide–carbide composites developed by alloyed melt infiltration. *J Eur Cer Soc* 2008; 28: 1267–1274.
23. Zhu Q and Shobu K. High-temperature fracture toughness of SiC-$Mo_5(Si,Al)_3C$ composites. *J Eur Cer Soc* 2000; 20: 1385–1389.
24. Ito K, Moriwaki M, Nakatomo T, et al. Plastic-deformation of single-crystals of transition-metal disilicide. *Mat Sci Eng A-Str Mat Prop Micro Proc* 1997; 233: 33–43.
25. Nakamura M. Elastic constants of some transition-metal-disilicide single crystals. *Metal Mat Trans A* 1994; 25A: 331–340.
26. Hansson T and Warren R. Particle and whisker reinforced brittle matrix composites. In: *Comprehensive composite material vol 4*. Oxford, UK: Elsevier Science Ltd., Cambridge University Press, 2000, pp. 579–609.
27. Eom JH, Kim YW and Jung BJ. Effect of alkaline earth additives on the flexural strength of silicon oxycarbide-bonded silicon carbide ceramics. *Cer Int* 2013; 39: 2083–2091.

28. Deng ZY, She J, Inagaki Y, et al. Reinforcement by crack-tip blunting in porous ceramics. *J Eur Cer Soc* 2004; 24: 2055–2059.
29. Lawn B. *Fracture of brittle solids*. New York, NY: Cambridge University Press, 1993, pp. 194–206.
30. Kulikovsky V, Vorlíček V, Boháč P, et al. Mechanical properties of amorphous and micro-crystalline silicon films. *Thin Solid Films* 2008; 516: 5368–5375.